Small-angle critical neutron scattering from cobalt

C. J. Glinka*†‡ and V. J. Minkiewicz*†§
University of Maryland, College Park, Maryland 20742

L. Passell‖
Brookhaven National Laboratory, Upton, New York 11973
(Received 14 January 1977)

Total and inelastic-neutron-scattering measurements have been made of the small-angle critical scattering from polycrystalline cobalt both above and below its Curie temperature T_C. Below T_C the scattering is dominated by well-defined spin-wave modes which exhibit quadratic dispersion, $\hbar\omega(q) = Dq^2$. Within the hydrodynamic region, the spin-wave stiffness constant is found to have the power-law temperature dependence $D \propto (T - T_C)^x$ where $x = 0.39 \pm 0.05$. As T_C is approached, the spin waves renormalize and broaden but no evidence of a central peak indicative of the longitudinal component of the susceptibility is observed. Above T_C, the exponents $\gamma = 1.23 \pm 0.05$ and $\nu = 0.65 \pm 0.04$, describing the power-law dependences of the static susceptibility and the inverse correlation range, respectively, have been obtained from the small-angle scans after taking full account of the inelasticity of the scattering. In addition, the critical scattering has been calibrated directly against the nuclear incoherent scattering and in this way the interaction range r_1, which appears in the classical and modified Ornstein-Zernike expressions for the asymptotic form of the spin pair correlation function, has also been determined. The linewidths of the quasielastic critical scattering have been measured over a range of wave vectors at temperatures up to 150°C above T_C. At T_C the linewidths vary with q to the 2.4 ± 0.2 power. Above T_C, the linewidths are well described by a dynamical scaling function which, however, differs from that previously found for iron.

I. INTRODUCTION

The scattering of thermal neutrons has proven to be a uniquely powerful tool for elucidating both the static and dynamic features of the critical fluctuations in magnetic systems. Among ferromagnetic materials, the techniques of neutron scattering have been applied most extensively to iron. From the resulting body of data on iron, a rather complete description of the critical scattering has emerged which is in good agreement with current theory in nearly all respects. The extent to which the detailed results obtained for iron are generally characteristic of isotropic ferromagnets is yet largely undetermined, however. This is particularly true with regard to the spin dynamics near T_C; the form of the dynamical scaling function which describes the temperature dependence of the lifetimes of the critical fluctuations has been measured for iron alone. The overall objective of the study described herein has been to examine in comparable detail the critical scattering from cobalt, to date the least studied of the $3d$-transition-metal ferromagnets. Both total and inelastic scattering measurements have been carried out to obtain the small-wave-vector and low-frequency dependence of the scattering function $S(\vec{Q}, \omega)$ in the critical region. Emphasis has been placed on inelastic-scattering measurements which have yielded the form of the dynamical scaling function above T_C. Although qualitatively similar, the scaling function for cobalt is notably different from that found for iron.

Previous studies of the critical behavior of cobalt have dealt solely with the static critical properties. Bulk measurements of the divergence of the uniform susceptibility above T_C by Colvin and Arajs,[1] Geissler and Lange,[2] and Rocker and Kohlhaas[3] place the value of the exponent γ at 1.20 ± 0.04. Such a low value for γ is to be contrasted with the results of similar measurements on iron and nickel which have yielded values for γ between 1.30 and 1.34. In the only reported measurement of the exponent β for cobalt, which describes the power-law temperature dependence of the spontaneous magnetization near T_C, Rocker and Kohlhaas[3] obtained $\beta = 0.42 \pm 0.01$. This result is supported, however, by the earlier magnetization measurements of Myers and Sucksmith,[4] which when plotted on a log-log scale give a value for β of 0.41. The consensus of numerous measurements of β for iron and nickel, on the other hand, is that $\beta = 0.38 \pm 0.01$ for both these materials. Hence, in bulk measurements of its static critical properties, cobalt has been observed to deviate from the behavior found for iron and nickel.

In the only previous study of the critical neutron scattering from cobalt, Bally *et al.*[5] measured the angular distribution of the small-angle scattering at several temperatures above T_C. Their results were analyzed within the static approximation in which the critical scattering is treated as entirely

elastic. Although they lacked data on the dynamics of the spin fluctuations on which to base such an approximation, they estimated that if the relaxation times of the spin fluctuations in cobalt were not less than those which had been measured for iron,[6] then inelasticity corrections to their data could be neglected. Within the static approximation, Bally *et al.* determined that $\gamma = 1.19$, in close agreement with the low values for γ derived from the bulk measurements. In addition, they extracted the inverse correlation range κ_1 from the angular distribution of the scattering and the exponent $\nu = 0.625$ for the dependence of κ_1 on the reduced temperature near T_C. This exponent is once again lower than that derived by Bally[7] in similar measurements on iron which gave $\nu = 0.70 \pm 0.015$.

Despite the apparent agreement between the neutron-scattering and bulk measurements of the static susceptibility, the underlying assumption of the neutron results that the dynamical behavior of the spin fluctuations is similar in iron and cobalt is open to question in light of the consistently different values obtained for the static critical exponents for the two materials. Furthermore, at the time of Bally's measurements there existed only limited data on the inelastic nature of the critical scattering from iron. Only subsequent experiments[8,9] revealed the extent to which inelasticity can affect the interpretation of total scattering data.[10] Hence in our study we have attempted to correlate measurements of the angular dependence of the critical scattering with extensive additional measurements of its energy dependence in order to quantitatively assess the importance of inelasticity corrections in the determination of the static critical exponents γ and ν.

Because cobalt undergoes a first-order structural transition from hcp to fcc at about 420 °C, only polycrystalline samples are conveniently available for studies near the critical point ($T_C = 1115$ °C). Critical-scattering measurements on cobalt are nonetheless feasible, if confined to the forward direction, for near T_C the magnetic scattering is expected to be isotropic at small scattering vectors. This is expected because cobalt is cubic in its high-temperature phase as are iron and nickel which experiments[8,11,12] on single crystals have shown to be magnetically isotropic near their respective critical points. Because of this magnetic isotropy, our measurements on cobalt have yielded a great deal of the information normally requiring single-crystal samples.

The remainder of this paper is organized as follows. In Sec. II we present various proposed forms for the neutron cross section near T_C in order to provide the theoretical background against which to view our results. In Sec. III we describe the experimental apparatus and the techniques used in making the measurements. Our experimental results are presented and discussed in Sec. IV. We note that some of these results have been briefly reported in two previous publications.[13] Finally, in Sec. V we compare the available experimental data regarding the critical behavior of cobalt with that for iron and nickel.

II. CRITICAL SCATTERING CROSS SECTIONS

A. General form of the cross section

The differential cross section for the scattering of unpolarized neutrons from an initial state $\vec{k}_i$ to a final state $\vec{k}_f$, with momentum transfer $\hbar\vec{Q} = \hbar(\vec{k}_i - \vec{k}_f)$ and energy loss $\hbar\omega = \hbar^2(k_i^2 - k_f^2)/2m_n$, by a system of N localized spins on a Bravais lattice is given by[14]

$$\frac{d^2\sigma}{d\Omega d\omega} = \hbar\left(\frac{\gamma e^2}{m_e c^2}\right)^2 \frac{k_f}{k_i} |F(\vec{Q})|^2 \sum_\alpha (1 - \hat{Q}_\alpha^2)\, \mathcal{S}^\alpha(\vec{Q}, \omega)\,, \tag{2.1}$$

where $F(\vec{Q})$ is the atomic magnetic form factor and $\mathcal{S}^\alpha(\vec{Q}, \omega)$, the so-called scattering law, is the spatial and temporal Fourier transform of the spin pair correlation function, i.e.,

$$\mathcal{S}^\alpha(\vec{Q}, \omega) = \frac{N}{2\pi\hbar} \sum_{\vec{R}} \int_{-\infty}^{\infty} dt\, e^{i(\vec{Q}\cdot\vec{R} - \omega t)} \langle S_0^\alpha(0) S_{\vec{R}}^\alpha(t)\rangle\,. \tag{2.2}$$

In (2.2), $S_{\vec{R}}^\alpha(t)$ is one Cartesian component of the spin operator at site $\vec{R}$ and time t. The term $(1 - \hat{Q}_\alpha^2)$ multiplying $\mathcal{S}^\alpha(\vec{Q}, \omega)$ in (2.1) selects those components of the scattering law which are perpendicular to the scattering vector $\vec{Q}$. For a polycrystalline sample, this term must be averaged over all possible crystallite orientations and is then equal to $\frac{2}{3}$. In this case all components of $\mathcal{S}^\alpha(\vec{Q}, \omega)$ contribute equally to the scattering.

Through the application of linear response theory,[15] it is possible to express the scattering law measured by neutron scattering in a form which separates the static and dynamic behavior of the spin correlations. This is accomplished through the introduction of two response functions, (i) $\chi^\alpha(\vec{Q})$, which is the susceptibility of the spin system to a static sinusoidal applied field of wave vector $\vec{Q}$, and (ii) a relaxation function $f^\alpha(\vec{Q}, t)$ which describes how the magnetization relaxes following the sudden cutoff at $t = 0$ of a steady-state field of periodicity $\vec{Q}$. A lucid account of how these two functions may be related to $\mathcal{S}^\alpha(\vec{Q}, \omega)$ is given in Ref. 14. Here we merely reproduce the general result for the complete wave-vector and frequency dependence of the scattering law

$$\mathcal{S}^{\alpha}(\vec{Q},\omega) = \mathcal{S}^{\alpha}_{\text{Bragg}}(\vec{Q},\omega=0) + \frac{NS(S+1)}{3\hbar}\frac{\hbar\omega\beta}{1-\exp(-\hbar\omega\beta)} \times \frac{\chi^{\alpha}(\vec{Q})}{\chi_0} F^{\alpha}(\vec{Q},\omega), \quad (2.3)$$

where $\chi_0 = \frac{1}{3}(g\mu_B)^2 S(S+1)\beta$ is the susceptibility of an isolated ion and the spectral-weight function $F^{\alpha}(\vec{Q},\omega)$ is the Fourier transform of the relaxation function $f^{\alpha}(\vec{Q},t)$, normalized such that

$$\int_{-\infty}^{\infty} F^{\alpha}(\vec{Q},\omega)\,d\omega = 1. \quad (2.4)$$

The first term in (2.3) is proportional to the square of the magnetization and gives rise to the elastic-magnetic Bragg scattering while the second term gives the diffuse, and in general inelastic, scattering from spin fluctuations which becomes the critical scattering near T_C. In this expression for $\mathcal{S}^{\alpha}(\vec{Q},\omega)$ the static properties of the spin fluctuations are manifested in $\chi^{\alpha}(\vec{Q})$ while $F^{\alpha}(\vec{Q},\omega)$ contains all the dynamical information. The wave-vector-dependent susceptibility $\chi^{\alpha}(\vec{Q})$ is defined such that $\chi^{\alpha}(\vec{Q}=0)$ is just the macroscopic isothermal susceptibility measured by bulk techniques.

By combining (2.3) with (2.1), we arrive at an expression for the diffuse cross section which is most convenient for discussing the magnetic scattering from an isotropic polycrystalline sample, namely,

$$\frac{d^2\sigma}{d\Omega d\omega} = \frac{2}{3}N\left(\frac{\gamma e^2}{m_e c^2}\right)^2 \frac{k_f}{k_i}|F(\vec{Q})|^2 \times S(S+1)\frac{\hbar\omega\beta}{1-\exp(-\hbar\omega\beta)} \times \left(\frac{1}{3}\frac{\chi^{l}(\vec{Q})}{\chi_0}F^{l}(\vec{Q},\omega) + \frac{2}{3}\frac{\chi^{t}(\vec{Q})}{\chi_0}F^{t}(\vec{Q},\omega)\right), \quad (2.5)$$

where the superscripts l and t identify, respectively, the longitudinal and transverse components of the susceptibility and spectral-weight functions defined with respect to the direction of the spontaneous magnetization, the only unique direction in an otherwise isotropic system.

B. Wave-vector-dependent susceptibility $\chi(\vec{Q})$

Above T_C, where the spontaneous magnetization is zero, no distinction can be made between transverse and longitudinal components of the susceptibility so that $\chi^{t}(\vec{Q}) = \chi^{l}(\vec{Q}) = \chi(\vec{Q})$. By applying the mean-field approximation to a Heisenberg ferromagnet, an expression for $\chi(\vec{q})$ valid for small values of the reduced scattering vector $\vec{q} = \vec{Q} - \vec{\tau}$ ($\vec{\tau}$ is a reciprocal-lattice vector) can be calculated and is found to have the familiar Ornstein-Zernike form

$$\chi(q) = \frac{\chi_0}{r_1^2(\kappa_1^2 + q^2)}. \quad (2.6)$$

$\chi(q)$ is related to the static pair correlation function by Fourier inversion[14] which, for the above expression, gives the well-known result

$$\langle \Delta S_0^{\alpha}(0)\,\Delta S_r^{\alpha}(0)\rangle = \frac{v_0}{12\pi}S(S+1)\frac{1}{r_1^2}\frac{e^{-\kappa_1 r}}{r}, \quad (2.7)$$

valid for large distances r. Here v_0 is the volume of the unit cell. It is through Eq. (2.7) that the parameter κ_1 receives its interpretation as an inverse correlation range and r_1, a measure of the strength of the spin correlations. Since $\chi(q=0)$ diverges as T_C is approached, Eq. (2.6) implies that $\kappa_1 = 0$ at T_C. The parameter r_1, however, is related to the range of direct interaction between individual spins and is expected to be only weakly temperature dependent through the critical point.

While the Ornstein-Zernike form for $\chi(q)$ has generally proven to give a good description of the critical scattering not only from magnetic systems but also from simple fluids and binary liquids and alloys, for example, small deviations from (2.6) have been observed experimentally[16] and predicted theoretically.[17] None of the various approximants for $\chi(q)$ which have been proposed, primarily by Fisher and coworkers,[18,19] will be mentioned here, however, for as will be shown in Sec. IV B the Ornstein-Zernike expression is entirely adequate to describe the small-angle critical scattering from cobalt above T_C.

Below T_C, the mean-field result in the small q limit for the longitudinal susceptibility $\chi^{l}(q)$ is once again of the Ornstein-Zernike form

$$\chi^{l}(q) = \frac{\chi_0}{r_1^2(\kappa_1^2 + q^2)}. \quad (2.8)$$

The q dependence obtained in this approximation for the transverse susceptibility $\chi^{t}(q)$ is simply,

$$\chi^{t}(q) = \frac{\chi_0}{r_1^2 q^2}. \quad (2.9)$$

Although small corrections to these two expressions have been proposed[20] based on theoretical approaches more sophisticated than mean-field theory, there is general agreement that $\chi^{t}(q)$ is not associated with an inverse correlation range which implies that only the longitudinal part of the susceptibility is expected to show divergent behavior as $T \to T_C$. This essential difference between $\chi^{l}(q)$ and $\chi^{t}(q)$ has been confirmed by recent experiments[21] on the nearly ideal isotropic Heisenberg ferromagnets EuO and EuS which are in

general accord with the mean-field expressions for $\chi^l(q)$ and $\chi^t(q)$ and provide about the best evidence to date for their validity, at least in describing a truly Heisenberg-like system.

C. Spectral weight function $F(q,\omega)$

In this section, we review some results for the spectral weight function obtained from spin-wave theory and the hydrodynamic theory of spin diffusion which serve to describe the dynamics well away from the critical point in the ordered and disordered phases, respectively. We then go on in Sec. II D to discuss how these results may be extended into the critical region with the aid of dynamical scaling and also mention the results of direct, though approximate, calculations of the time-dependent spin correlation function near T_C.

In the ordered state, the transverse fluctuations of the magnetic moments are spin waves which for an isotropic ferromagnet exhibit quadratic dispersion, $\hbar\omega(q) = \pm Dq^2$, in the small q limit. The spectral-weight function obtained from linear spin-wave theory at low temperatures consists of sharp peaks at the spin-wave creation and annihilation energies. At higher temperatures the effects of spin-wave interactions become important and result in the renormalization of the spin-wave energies and in the reduction of the spin-wave lifetimes.[22] Correspondingly, the sharp peaks in the spectral weight function broaden and shift to lower energies. The most commonly proposed form for the spectral weight function which incorporates these effects consists of a pair of Lorentzian line shapes,

$$F^t(q,\omega) = \frac{1}{2\pi}\left(\frac{\Gamma}{[\omega-\omega(q)]^2+\Gamma^2} + \frac{\Gamma}{[\omega+\omega(q)]^2+\Gamma^2}\right), \tag{2.10}$$

where Γ is, in general, a q-dependent damping constant inversely related to the spin-wave lifetime. Here, the spin-wave dispersion still has the form $\hbar\omega(q) = Dq^2$, but now the so-called stiffness constant D is temperature dependent.

An alternative spectral-weight function has been proposed by Halperin and Hohenberg[23] based on hydrodynamic theory. They suggest

$$F^t(q,\omega) = \frac{1}{\pi}\frac{\gamma\omega(q)^2}{[\omega^2-\omega(q)^2]^2+\gamma^2\omega(q)^2}, \tag{2.11}$$

where $\gamma(q)$ is a damping constant. This form for $F^t(q,\omega)$ also has peaks at $\pm\omega(q)$ and differs in shape from the double Lorentzian form only when the spin-wave peaks partially overlap which occurs when the damping becomes comparable to $\omega(q)$. In this limit, the validity of either expression is questionable, however, for one assumption of the hydrodynamic theory underlying equation (2.11) is that $\gamma \ll \omega(q)$.

At temperatures where linear spin-wave theory begins to break down, longitudinal fluctuations in the magnetization are expected to play an increasingly important role in the dynamics. For the most part, theory and experiment have agreed that the longitudinal fluctuations show nonpropagating, diffusivelike behavior; the most commonly proposed form for $F^l(q,\omega)$ being a single Lorentzian centered at $\omega = 0$. Such a central peak is expected to become more pronounced as the temperature is raised (ultimately to diverge at T_C for $q = 0$) and to have an integrated intensity which varies as q^{-2} in accord with the expression for $\chi^l(q)$ in Eq. (2.8). These expectations have been borne out in experiments on isotropic[9] and anisotropic[24] antiferromagnets and on anisotropic ferromagnets,[25] but repeated attempts to observe a central peak in the isotropic ferromagnets Fe,[8,26] Ni,[12] and EuS and EuO,[27] have yielded null results. There have been two recent experiments, one[28] on Fe and the other[29] on the nearly isotropic metallic ferromagnet CoS_2, in which some indication of a weak central peak was observed immediately below T_C, but in neither case could the scattering be positively identified as arising from the longitudinal fluctuations.

In what is perhaps the most thorough treatment of the longitudinal spin fluctuations in a ferromagnet below T_C, Vaks *et al.*[30] have suggested that the longitudinal fluctuations can decay through interaction with the spin waves. They describe a process of spin diffusion through spin waves which they argue is enhanced in an isotropic ferromagnet because the Dq^2 dispersion relation implies a high density of long-wavelength spin-wave states to promote the interaction. In their calculations based on the Heisenberg model, they find that in addition to a small central peak, $F^l(q,\omega)$ should also have sidebands which peak at the spin wave energies $\omega(q) = \pm Dq^2$. If, in fact, much of the longitudinal spectral weight is concentrated in sideband peaks, then this could explain why the observation of a central peak has proven so difficult.

At the other end of the temperature scale, well above T_C, the spin system is homogeneous to a high degree owing to the nearly complete disorder of the moments and therefore hydrodynamic theory is once again applicable for analyzing at least the long-wavelength low-frequency phenomena. Van Hove first suggested[31] that in this regime the magnetization density $\vec{M}(\vec{r},t)$ obeys a diffusion equation of the form $d\vec{M}/dt = \Lambda\nabla^2\vec{M}$ where $\Lambda(T)$ is the spin diffusion constant. Accordingly, an initial plane wave of magnetization of wave vector q decays in time like $\exp(-\Lambda q^2 t)$. The Fourier trans-

form of this relaxation function gives the spectral weight function

$$F(q,\omega)=\frac{1}{\pi}\frac{\Lambda q^2}{(\Lambda q^2)^2+\omega^2}. \tag{2.12}$$

There is a basic agreement on the above form for $F(q,\omega)$ in the high-temperature low-q limit both from more microscopic theories and from a number of experiments.

D. Dynamical scaling

The results presented in the previous section, obtained from hydrodynamic theory, are valid for long wavelengths and low frequencies. According to the concepts of static scaling originally put forth by Widom,[32] Kadanoff,[33] and others,[34] all lengths should be measured relative to the correlation range $\xi=\kappa^{-1}$ since it is assumed that ξ reflects the most important effects of critical fluctuations. In this view, hydrodynamic theory should apply at temperatures and wave vectors such that $\kappa/q\gg1$, while quite different behavior can be expected in the so-called critical region where $\kappa/q\ll1$.

The static-scaling hypothesis assumes that a single function describes the spin correlations for all q and κ, with a characteristic dependence on the ratio κ/q. Expressed mathematically, the static-scaling hypothesis states that the static-pair correlation function is a homogeneous function of κ and q, which implies that the static susceptibility can be written in the form $\chi(q)\propto q^{y}h(\kappa/q)$. Note that the expressions for $\chi(q)$ given in Sec. II B can be cast in this form where the exponent $y=-2$.

Scaling arguments were first extended to dynamic phenomena by Ferrell *et al.*[35] in connection with the superfluid transition in helium and later reformulated by Halperin and Hohenberg[23] for magnetic systems. They proposed that there is a characteristic frequency which plays an analogous role in describing the dynamics of the spin fluctuations that the characteristic length, the correlation range, does for the statics. Thus they suggest that the spectral-weight function has the form

$$F(q,\omega)=\frac{1}{\omega_\kappa(q)}f_{\kappa,q}(\omega/\omega_\kappa(q)), \tag{2.13}$$

where the factor $\omega_\kappa(q)^{-1}$ insures the normalization $\int_{-\infty}^{\infty}f_{\kappa,q}(x)\,dx=1$. In Eq. (2.13), the characteristic frequency $\omega_\kappa(q)$ is defined by the relation

$$\int_{-\omega_\kappa(q)}^{\omega_\kappa(q)}F(q,\omega)\,d\omega=\tfrac{1}{2}, \tag{2.14}$$

and thus half the area under $F(q,\omega)$ lies within $\pm\omega_\kappa(q)$. This definition of $\omega_\kappa(q)$, although admittedly arbitrary, has a precise meaning at all temperatures regardless of the shape of $F(q,\omega)$.

Underlying dynamical scaling is the assumption that not only the static but the frequency-dependent correlation function depends crucially on the ratio κ/q. This assumption is expressed in two specific hypotheses, namely: (i) that the characteristic frequency $\omega_\kappa(q)$ is a homogeneous function of q and κ,

$$\omega_\kappa(q)=\sigma q^{z}\Omega(\kappa/q) \tag{2.15}$$

and (ii) that the scaled spectral-weight function $f_{\kappa,q}(\omega/\omega_\kappa(q))$ depends only on the ratio κ/q and not on q or κ separately. Thus the shape of $F(q,\omega)$ will be the same, apart from a change of scale, for all values of q and κ such that the ratio κ/q is fixed.

The dynamical scaling hypotheses can be used to relate the behavior of the spin dynamics in the critical region to that in the hydrodynamic regions above and below the critical point. For example, in the spin-wave region below T_C it can be shown from hydrodynamic theory[23] that the stiffness constant D is proportional to $\kappa^{1/2}$ so that the complete temperature and wave-vector dependence of the characteristic frequency in this region is given by[36]

$$\omega_\kappa(q)=Dq^2\propto\kappa^{1/2}q^2,\quad \kappa\gg q,\quad T<T_C. \tag{2.16}$$

Comparing this with the general form for $\omega_\kappa(q)$, Eq. (2.15) implies that $\Omega(\kappa/q)\to(\kappa/q)^{1/2}$ in this limit and therefore the exponent $Z=\frac{5}{2}$. These conclusions in turn imply that at T_C, where $\kappa=0$ and so $\Omega(\kappa/q)$ is a constant for all q, the characteristic frequency is simply

$$\omega_\kappa(q)=\sigma q^{5/2},\quad T=T_C, \tag{2.17}$$

where for convenience we have let $\Omega(0)=1$.

Although important features of the critical behavior may be inferred from hydrodynamic theory through dynamical scaling, scaling itself does not predict the functional form of the correlation function. To do so requires a microscopic theory. Hubbard[37] has recently succeeded in extending the work of Mori,[38] Kawasaki,[39] and others,[40] to calculate approximately the time-dependent spin correlation functions in the paramagnetic and critical regions for an isotropic Heisenberg model with nearest-neighbor coupling. From these results he has been able to predict the inelastic neutron scattering line shapes and widths at all temperatures above T_C. The spectral-weight function he obtains does not have a simple analytical representation, however, but must be calculated numerically. Figure 1 shows the results of such a numerical calculation in which the normalized spectral-weight function $F(q,\omega)/F(q,0)$ is plotted versus the scaled frequency $\omega/\sigma q^{5/2}$ for various values of κ/q. The first point to be noted from Fig. 1 is that the shape of $F(q,\omega)$ depends

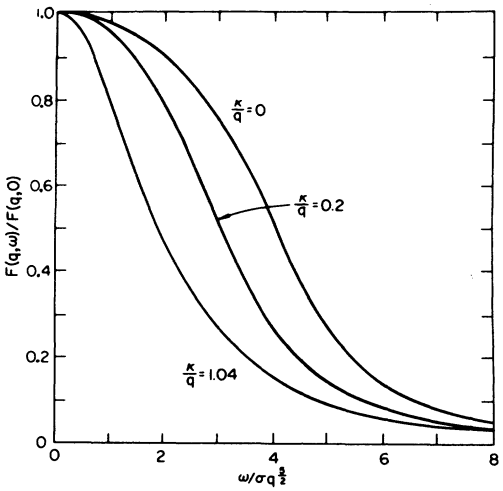

FIG. 1. Normalized spectral-weight function calculated by Hubbard for the simple cubic Heisenberg ferromagnet with nearest-neighbor coupling. When plotted vs the scaled frequency $\omega/\sigma q^{5/2}$, the spectral function depends only on the ratio κ/q in agreement with the dynamical scaling hypotheses (from Ref. 37).

only on the ratio κ/q as anticipated by dynamical scaling. Furthermore, the widths of the curves in Fig. 1 are evidently of the form given in Eq. (2.15) with $Z=\frac{5}{2}$. Thus the predictions of dynamical scaling are contained in the results of Hubbard's calculations. The other significant feature shown in the figure is the progressive change in the shape of $F(q,\omega)$ from a rounded, Gaussian-like line at $T_C(\kappa/q=0)$ to the Lorentzian shape $F(q,\omega)$ must take at large values of κ/q. A distinctly non-Lorentzian shape at T_C, similar to that in Fig. 1, has generally been observed for isotropic ferromagnets.[8,12,27]

III. EXPERIMENTAL APPARATUS AND PROCEDURES

The measurements to be presented in Sec. IV were performed on a triple-axis spectrometer at the High-Flux Beam Reactor at Brookhaven National Laboratory. Pyrolytic graphite crystals were used as monochromator and analyzer and all measurements were made with a filtered incident beam of 13.5 meV ($\lambda=2.46$ Å). For most of the inelastic scattering measurements, Soller slit collimators with horizontal divergence angles of 20-10-20-20 minutes were used in the in-pile, monochromator-to-sample, sample-to-analyzer, and analyzer-to-detector regions, respectively, resulting in a measured energy resolution of 0.37 ±0.02 meV (full width at half-maximum).

Measurements of the angular dependence of the critical scattering were carried out by operating the spectrometer in the two-axis mode in which the analyzer crystal is removed and thus all neutrons scattered through a given angle are detected regardless of their energies. For these measurements, Q resolution is of utmost importance and the increased intensity resulting from removal of the analyzer crystal permits tighter Q resolution to be imposed. In addition to horizontal collimation having divergence angles of 20-20-20 min, Soller slit assemblies with a vertical divergence of 40 min were inserted before and after the sample. The vertical Q resolution of this configuration, which gives the largest contribution to the overall resolution, was measured to be 0.045 ± 0.02 Å^{-1}. By contrast, the Q resolution along the scattering vector was 0.020 Å^{-1}.

An aluminum vacuum furnace provided access to the high temperatures needed for the critical scattering measurements ($T_C=1115$ °C). The sample was heated by direct radiation from a graphite resistance heater specially designed to produce no magnetic field at the sample position. The temperature distribution in the hot zone was tested by measuring the peak in the critical scattering as a function of temperature, first from the top of the sample and then from the bottom. The total temperature difference across the face of the sample was thus estimated to be about 1° at 1100 °C. The furnace temperature was regulated with a three-mode temperature controller which enabled temperature variations to be held to less than 0.5 °C over a period of 24 h.

The polycrystalline samples used in our measurements were thin slabs 38×32×2 mm owing to cobalt's rather large absorption cross section of nearly 52 b for 13.5 meV neutrons. Because cobalt has a considerable vapor pressure near its Curie point, it was necessary to encapsulate the samples to prevent loss of material through evaporation. Sample containers of aluminum oxide were fabricated for this purpose and the platinum-rhodium thermocouples used to monitor the temperature were affixed to the containers to prevent their alloying with the samples. This arrangement precluded absolute temperature measurements, however temperatures relative to the Curie point could be accurately determined by calibrating each thermocouple from the peak in the critical scattering, as mentioned above. Considering all sources of uncertainty, the precision with which temperature differences, $|T-T_C|$, could be determined was about 1.5 °C.

IV. EXPERIMENTAL RESULTS AND DISCUSSION

A. Dynamics below T_C—spin waves

We choose to present first the results of our inelastic scattering measurements below T_C. Owing

to the extreme steepness of the spin-wave dispersion in cobalt ($D = 385$ meV Å^2 for cobalt[41] stabilized in the fcc phase at room temperature) plus the limited range of energy transfer available in a small-angle experiment, our observations of the spin waves were restricted to temperatures close to T_C, where their energies are greatly reduced as a result of spin-wave renormalization. Below about 1000 °C, triple-axis constant-Q scans reveal only an elastic temperature-independent peak arising from cobalt's rather large (5.9 b) nuclear spin-incoherent cross section. Careful scans of this nonmagnetic contribution to the scattering were subsequently subtracted from the data in the critical region. Despite the rather large incoherent cross section, the nonmagnetic scattering amounted to only one or two percent of the total at T_C.

We were able to observe the spin waves for wave vectors $0.03 \leq q \leq 0.08$ Å^{-1} over the temperature range $0.002 \leq 1 - T/T_C \leq 0.03$; at lower temperatures the spin-wave peaks lie beyond the available range of energy transfer and at larger wave vectors the spin waves are too severly broadened to be identifiable as discrete excitations. In Fig. 2, the intensity recorded in constant-Q scans taken at 8° below T_C ($1 - T/T_C = 0.006$) is plotted versus neutron energy transfer. At each wave vector distinct spin-wave creation and annihilation peaks are seen which exhibit dispersion and a significant q-dependent line broadening. Each scan in the figure extends over the entire range of energy transfer accessible at that wave vector.

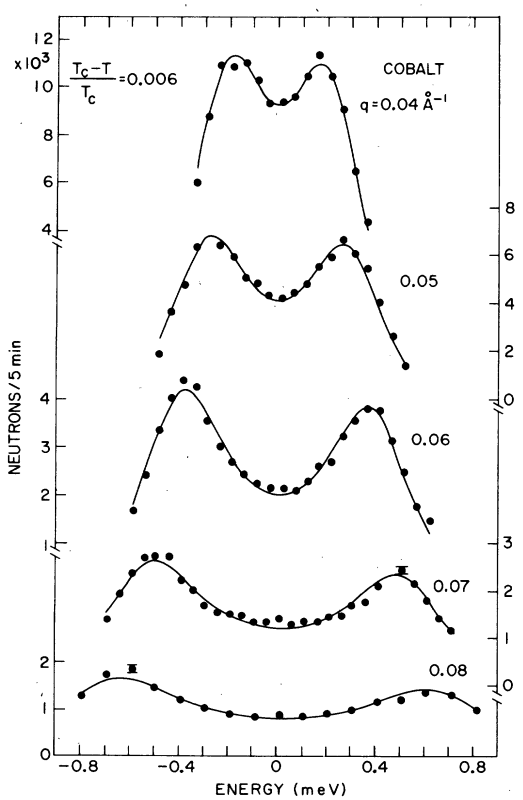

FIG. 2. Spin-wave line shapes observed in constant-Q scans at 8 °C below T_C. The solid curves were obtained by convoluting the Halperin-Hohenberg spin-wave cross section with the spectrometer resolution function.

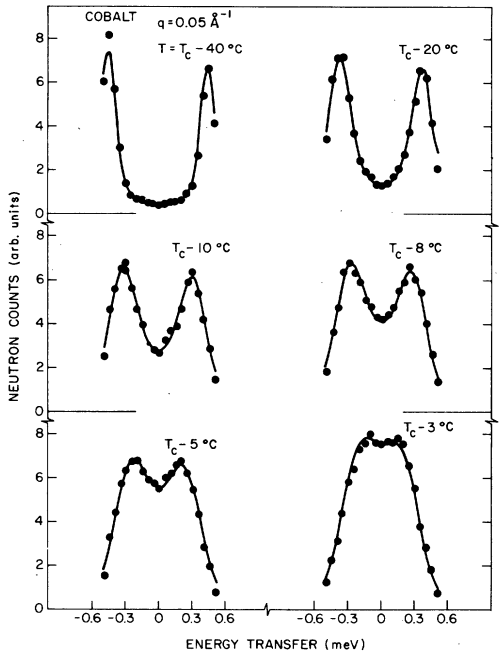

FIG. 3. Spin-wave line shapes observed in constant-Q scans for $Q = 0.05$ Å^{-1} at several temperatures below T_C. The curves in the figure are least-squares fits to the data obtained using Halperin-Hohenberg form for the cross section.

The renormalization and broadening of the spin waves is illustrated in Fig. 3 which shows line shapes observed at a fixed q of 0.05 Å^{-1} for several temperatures. At the lowest temperature, where the spin waves are just coming into view, their widths are due solely to instrumental resolution. This indicates that the spin-wave dispersion at small wave vectors is truly isotropic for if it were not, the implicit averaging over all directions in the Brillouin zone inherent in measurements on polycrystalline samples would introduce a width over and above that due to other sources. We also note that there is no indication in either Fig. 2 or 3 of a central peak due to the longitudinal susceptibility. We shall consider this point further later in this section.

In an attempt to account in detail for the spin-wave line shapes we observed as well as obtain resolution-corrected values for the spin-wave energies, we fit all of our data using both the

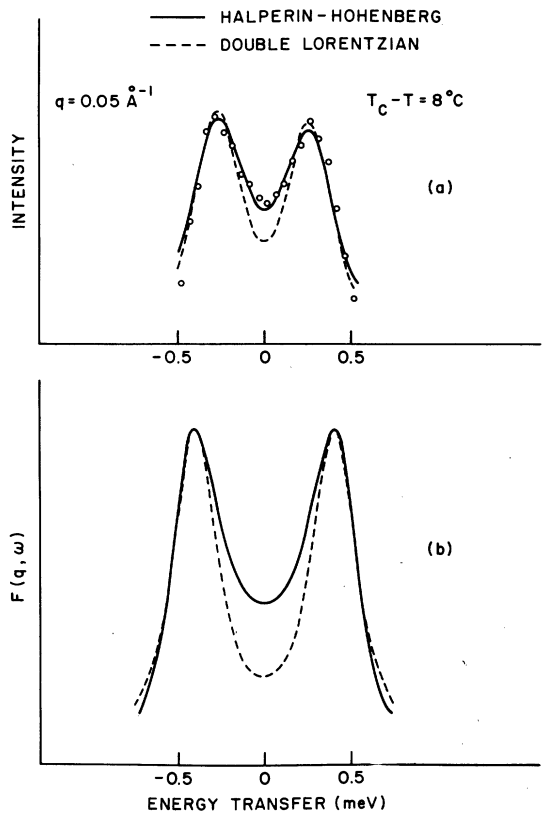

FIG. 4. (a) Results of fitting both the Halperin-Hohenberg and double Lorentzian forms of the spectral-weight function to a typical spin-wave line shape; (b) the two forms for $F(q,\omega)$ are contrasted more directly by matching their peak heights and half-widths.

double Lorentzian [Eq. (2.10)] and Halperin-Hohenberg [Eq. (2.11)] forms for the spectral-weight function together with Eq. (2.9) for the transverse susceptibility. An overall scale parameter, the spin-wave energy and the damping constant in each cross section were treated as variables to be determined by the nonlinear least-squares fitting routine. In those few instances where the spin waves are well separated, the two forms of the cross section are virtually indistinguishable and give equally satisfactory fits to the data. When the spin-wave peaks partially overlap, however, the Halperin-Hohenberg spectral function provides a systematically better fit to the line shape as a whole, particularly around $\omega = 0$. This point is brought out in Fig. 4(a) which shows the results of fitting the profile observed for $q = 0.05$ Å^{-1}, taken at 8° below T_C, to both the double Lorentzian (dashed curve) and Halperin-Hohenberg (solid curve) spectral functions, folded with the resolution function. The double Lorentzian curve, forced to fit the spin-wave peaks, is seen to fail to account for all the intensity near $\hbar\omega = 0$. The Halperin-Hohenberg (HH) curve, on the other hand, is quite adequate in describing the entire line shape. The two cross-sectional forms are contrasted more directly in Fig. 4(b) where the spectral functions, not folded with the resolution function, are plotted such that their peak and half-height positions coincide. The double Lorentzian curve falls below the HH curve at $\hbar\omega = 0$ but rises above it in the wings.

The solid curves in Figs. 2 and 3 were obtained by convoluting the HH cross section with the resolution function. The line shapes in these figures, and all of our spin-wave data, are well represented in this way.

That the two-peaked HH spectral-weight function is so successful in representing the entirety of our spin-wave data, right up to T_C, is surprising since it is expected to apply only within the low-temperature hydrodynamic regime. In fact, if the criterion of the hydrodynamic region that the spin-wave damping be much smaller than the spin-wave frequency, $\gamma \ll \omega(q)$, is not satisfied, then the HH expression [Eq. (2.11)] is not even properly normalized, i.e., integrating over all frequencies gives,

$$\int_{-\infty}^{\infty} F_{\mathrm{HH}}(q,\omega)\, d\omega = (\rho+1)^{1/2}/(2\rho)^{1/2}, \tag{4.1}$$

where $\rho = \{1+[\gamma/\omega(q)]^2\}^{1/2}$. Only when $\gamma \ll \omega(q)$ does the right-hand side of Eq. (4.1) approach unity. And yet when the HH spectral function is multiplied by $(2\rho)^{1/2}/(\rho^2+1)^{1/2}$, so that it is normalized for all values of γ and $\omega(q)$, the overall scale parameter determined by our fitting routine is nearly constant for all the line shapes at a given temperature. This is significant because it indicates that the presumed form for the transverse susceptibility, $\chi^t(q) \propto q^{-2}$, can account for the large variation of spin-wave intensity with wave vector that can be seen in Fig. 2, for example. In other words, a cross section consisting of a static term proportional to q^{-2} and the HH form, properly normalized, for the spectral-weight function is sufficient to describe both the frequency and q dependence of the inelastic scattering line shapes we observed below T_C. The overall normalization constant obtained by fitting to our spin-wave data did show a gradual temperature dependence, however, increasing as T_C is approached. This could perhaps indicate the presence of a broad central peak although without further evidence this is only speculation.

The resolution-corrected spin-wave energies obtained from our fitted line shapes follow a quadratic dispersion relation, $\hbar\omega(q) = Dq^2$. Yet derived values for the stiffness constant D, when plotted versus reduced temperature on a log-log scale, show systematic deviation, near T_C, from the

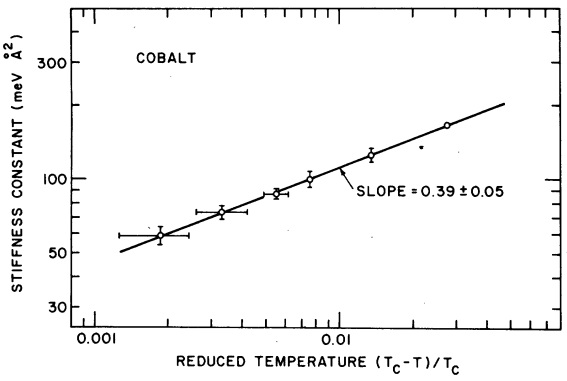

FIG. 5. Spin-wave stiffness constant D plotted vs $(1-T/T_C)$ on a log-log scale. The values for D were derived from only those data estimated to lie within the hydrodynamic region.

simple power-law temperature dependence expected from hydrodynamic theory. This may result because most of our data fail to satisfy the criterion that $\gamma \ll \omega(q)$ and so probably lie outside the hydrodynamic regime. However, if we ignore those data which grossly violate this criterion and plot values for D obtained from only those data which satisfy the weaker, and admittedly arbitrary, condition $\gamma/\omega(q) \leq 1$, we then do find a simple power-law temperature dependence. This is shown in Fig. 5 where we find that, treated in this way, the data yield a stiffness constant which varies as the 0.39±0.05 power of the reduced temperature. Hydrodynamic theory, together with static scaling,

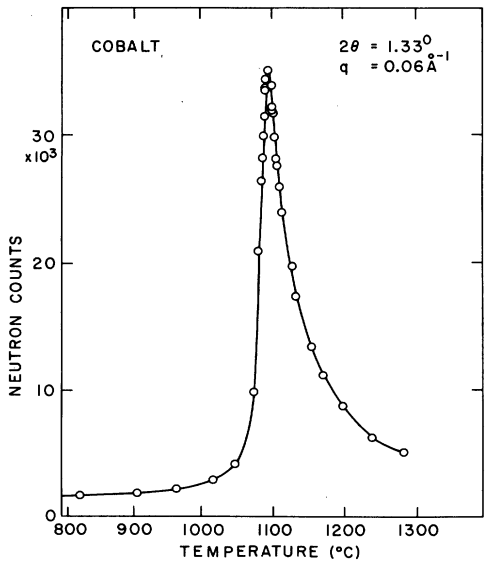

FIG. 6. Total scattered intensity observed at a fixed scattering angle of 1.33° as a function of temperature. The peak in the scattering served to locate the Curie point to within 1 °C.

predicts[23] the value of this exponent to be equal to $\nu' - \beta$, where ν' and β are exponents describing, respectively, the temperature dependence of the inverse correlation range and the magnetization. According to static scaling, $\nu' = \nu$ (the corresponding exponent above T_C) and series-expansion calculations for the Heisenberg model estimate[19] the exponent ν to be ~0.70 and[42] the exponent β to be ~0.38 so that $\nu' - \beta \sim 0.32$, which is somewhat lower than the exponent we obtain.

We conclude this section by returning to the puzzling problem of identifying the scattering associated with the longitudinal susceptibility which is presumably the true, i.e., divergent, critical scattering. Figure 6 shows the result of a two-axis measurement of the total scattering observed at a fixed scattering angle of $2\theta = 1.33°$ ($q = 0.06$ Å^{-1}) as a function of temperature. From the intense, well-defined peak seen in the total scattering, we were able to locate the Curie temperature to within 1 °C. Since in a two-axis experiment, neutrons with all values of scattered wave vector k_f (and hence all values of energy transfer $\hbar\omega$ from $-\infty$ to $\hbar^2 k_i^2/2m$) are detected, it might at first seem that the spin waves would give some contribution to the observed intensity at all temperatures below T_C. The sharp rise in intensity near T_C would then seem to be clear evidence for the diverging longitudinal susceptibility. However, in order to observe scattering from a spin wave with energy $\hbar\omega = Dq^2(\omega)$ [the dependence of q on ω for a fixed scattering angle 2θ is given in Eq. (4.3)] in a two-axis experiment, the energy conservation condition $\hbar\omega = (\hbar^2/2m)(k_i^2 - k_f^2)$ must, of course, also be satisfied, and together these two conditions do restrict the observability of the spin-wave scattering for a material like cobalt. For the circumstances under which the data in Fig. 6 were recorded ($k_i = 2.55$ Å^{-1}, $2\theta = 1.33°$), these two equations for $\hbar\omega$ have simultaneous solutions only for $0 \leq D \leq 90$ meV Å^2. The spin-wave dispersion in cobalt stiffens so rapidly that $D = 90$ meV Å^2 at about 10 °C below T_C. Consequently, even in a two-axis measurement, the spin waves contribute to the scattered intensity only in the immediate vicinity of T_C. The sharp peak in Fig. 6 is, therefore, at least partially due to the transverse rather than the longitudinal fluctuations.

In order to estimate the spin-wave contribution to the line shape in Fig. 6, we integrated the double-differential cross section which best described our triple-axis measurements over the path in q, ω space corresponding to the fixed scattering angle $2\theta = 1.33°$. We performed the integration numerically, using, below T_C, only the expression for the transverse susceptibility [Eq. (2.9)] and the HH form for the transverse spectral-

weight function. The temperature dependence of the cross section enters primarily through the stiffness constant which was taken to be $D = 680(1 - T/T_C)^{0.39}$ meV Å^2 as derived from our triple-axis measurements, and secondarily through the spin-wave line width γ which was taken to be proportional to $(1 - T/T_C)^{-1}$ as predicted by scaling.[23] Above T_C, the spectral function deduced from our triple-axis data (Sec. IV D) was used in the calculation along with the Ornstein-Zernike susceptibility, including the temperature dependence of κ_1 derived from our angular scans (Sec. IV B). The results of our numerical calculations are shown as the dashed curve in Fig. 7 where the intensities computed with the two forms for the cross section have been smoothly joined at T_C. The curve in Fig. 7 is seen to reproduce quite closely the data in Fig. 6 considering that no more than qualitative agreement can be expected from the approximate cross-sectional forms used in the calculation (the exact shape of the foot of the curve below T_C depends on the detailed wave vector and temperature dependence of the spin-wave linewidths, for example). This basic agreement with the data in Fig. 6 allows us to draw two conclusions regarding the critical scattering below T_C. First of all, we see that, just as with our triple-axis measurements, the critical scattering observed in Fig. 6 can be satisfactorily accounted for solely in terms of the cross section for the transverse susceptibility. It

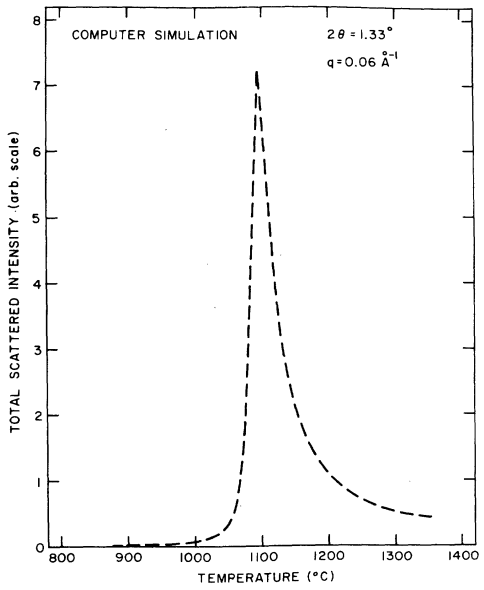

FIG. 7. Result of numerically integrating the differential cross section derived from triple-axis measurements so as to simulate the total scattering observed at a fixed scattering angle as a function of temperature. The figure is to be compared with the experimental curve shown in Fig. 6.

may be that the form of the cross section for the longitudinal susceptibility is not greatly different from that for the transverse susceptibility, at least over the wave vector and temperature range of our measurements, as suggested by Vaks *et al.*[30] And secondly, Fig. 7 reveals that, as a consequence of the steepness of the spin-wave dispersion in cobalt, at temperatures well below T_C there is no magnetic scattering whatsoever near the forward direction. This is significant because the ability to separate the magnetic scattering from that due to other sources is a crucial, although often underemphasized, factor in the determination of critical exponents. Figure 7 implies that, for cobalt, the background contribution to either two-axis or triple-axis scans made in the critical region may be simply determined by making corresponding scans at 800 °C, for example.

B. Wave-vector-dependent susceptibility and inverse correlation range above T_C

Above T_C, the critical scattering is quasielastic and can be associated with a single expression for the static susceptibility $\chi(q)$ and spectral function $F(q,\omega)$. For both these reasons the critical scattering above T_C is more amenable to detailed, quantitative study by small-angle scattering than that below T_C.

In order to determine the static susceptibility $\chi(q)$ and inverse correlation range κ_1, the angular distribution of the scattering was measured in a series of double-axis scans at temperatures up to 150 °C above T_C. As already noted, in the two-axis mode the spectrometer implicitly integrates over all neutron energy transfers corresponding to scattering through a fixed angle θ. As a result, the cross section which is directly measured[10] becomes [from Eq. (2.3)]

$$\sigma(\theta) \propto \int_{-\infty}^{\hbar k_i^2/2m} \left[k_i^2 - \left(\frac{2m}{\hbar}\right)\omega\right]^{1/2} \left(\frac{\beta\hbar\omega}{1-e^{-\beta\hbar\omega}}\right) \times \hat{\chi}(q)\, F(q,\omega)\, d\omega\,, \tag{4.2}$$

where q is a function of the energy transfer $\hbar\omega$ through the relation

$$q(\omega) = \left\{2k_i^2 - \left(\frac{2m}{\hbar}\right)\omega - 2k_i\left[k_i^2 - \left(\frac{2m}{\hbar}\right)\omega\right]^{1/2}\cos\theta\right\}^{1/2}. \tag{4.3}$$

The first factor in the integrand of Eq. (4.2) arises because $(d^2\sigma/d\Omega d\omega)$ is proportional to k_f/k_i while the second factor is the detailed balance factor with $\beta = 1/k_B T$. If the spectral function $F(q,\omega)$ is a narrow function of ω, i.e., the scattering is nearly elastic, or if k_i is large so that $q(\omega)$ is nearly constant, the cross section $\sigma(\theta)$ in Eq. (4.2) becomes

simply proportional to the reduced susceptibility $\hat{\chi}(q) \equiv \chi(q)/\chi_0$. When either of these conditions obtains, the angular dependence of the scattering may be analyzed solely in terms of $\hat{\chi}(q)$. This is known as the quasistatic approximation. In general, however, knowledge of $F(q,\omega)$ is necessary to infer $\hat{\chi}(q)$.

In order to obtain direct information regarding the inelasticity of the scattering above T_C, a separate series of triple-axis scans were undertaken in which the frequency distribution of the scattering at fixed wave vectors was determined. These measurements, to be described in Sec. IV D, served to characterize $F(q,\omega)$ over the wave vector and temperature range of our two-axis data. The frequency dependence of $F(q,\omega)$ was found to be well represented, except in the immediate vicinity of T_C, by a single Lorentzian, peaked at $\omega = 0$. This simple shape, plus the fact that $F(q,\omega)$ is a normalized function, reduced the task of specifying $F(q,\omega)$ to one of empirically determining its Lorentzian width $\Gamma(q)$ as a function of wave vector and temperature. By measuring $\Gamma(q)$ at several temperatures, we were able to approximate its functional dependence with simple analytic expressions which were in turn used to interpolate between the measured points to obtain $\Gamma(q)$ at general values of q and T.

With the form of $F(q,\omega)$ deduced from our triple-axis measurements, we were able to correct our two-axis data for the effects of inelasticity in the following manner.[43] First, the integral in Eq. (4.2) is evaluated numerically using a Lorentzian $F(q,\omega)$ and a parametrized form for $\hat{\chi}(q)$. For example, if the Ornstein-Zernike expression, $\hat{\chi}^{-1}(q) \propto q^2 + \kappa_1^2$, is used, then $\sigma(\theta)$ depends only on the parameter κ_1. Using a least-squares routine, a search is made for the value of κ_1 for which the computed constant-angle cross sections are simply proportional to the measured intensities, $I(q) = C\sigma(\theta,\kappa_1)$, for all angles θ. The success of this procedure depends, of course, on choosing the correct form for $\hat{\chi}(q)$ in evaluating $\sigma(\theta,\kappa_1)$.

Having determined the value of κ_1 for a given temperature, it is convenient to compute the so-called inelasticity correction factor, $R(q,\kappa_1)$, defined as

$$R(q,\kappa_1) = \sigma(\theta,\kappa_1)/\sigma(q,\kappa_1), \tag{4.4}$$

where $\sigma(q,\kappa_1)$ is obtained from Eq. (4.2) by replacing $F(q,\omega)$ with a δ function, i.e., $\sigma(q,\kappa_1)$ is the two-axis cross section in the limit that the scattering is entirely elastic. Corrected values for the two-axis intensities are then computed by dividing the measured intensities by $R(q,\kappa_1)$,

$$I_{\text{elas}}(q) = I(q)/R(q,\kappa_1) = C\sigma(q,\kappa_1). \tag{4.5}$$

Ideally, therefore, the corrected intensities are those that would be observed if the scattering were totally elastic. Since $\sigma(q,\kappa_1) \propto \hat{\chi}(q)$, the corrected intensities should exhibit the functional dependence of the assumed form for $\hat{\chi}(q)$; this is the ultimate criterion for judging the success of the correction procedure.

In addition to corrections for inelasticity, our two-axis data were further corrected for the effects of finite instrumental resolution. This amounts to performing a weighted average of the cross section over the region in q space sampled by the spectrometer. We combined corrections for inelasticity and resolution in one calculation by folding both $\sigma(\theta,\kappa_1)$ and $\sigma(q,\kappa_1)$ with the resolution function before forming the inelasticity correction factors $R(q,\kappa_1)$. Owing to the tight collimation conditions employed in our two-axis measurements, the resolution corrections were not large, amounting to only a few percent adjustment in the observed intensities.

The results of correcting our two-axis data for inelasticity and resolution effects are illustrated in Figs. 8 and 9. In Fig. 8 the uncorrected, reciprocal intensities (open circles) measured in a typical angular scan at 35 °C above T_C are plotted as a function of q^2. Also shown in the figure are these same reciprocal intensities (filled circles) corrected for inelasticity and resolution effects assuming an Ornstein-Zernike form for $\hat{\chi}(q)$. The raw data are seen to deviate substantially from the straight-line, Ornstein-Zernike-like behavior obeyed by the corrected intensities. The deviations, which are almost entirely due to inelasticity rather than resolution effects, are most pronounced at the larger q's where the scattering is most inelastic, the width $\Gamma(q)$ of the spectral-weight function increasing roughly with q^2.

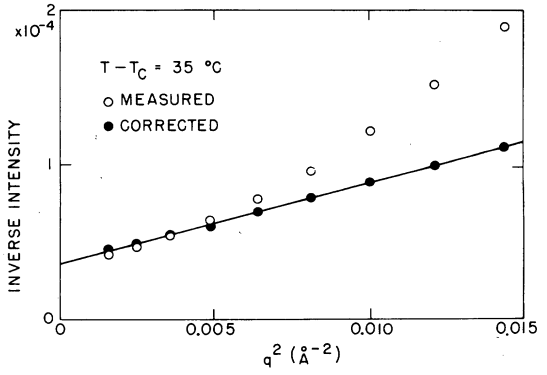

FIG. 8. Open circles are the reciprocal total scattering intensities observed at 35 °C above T_C plotted vs q^2. The filled circles are obtained from the measured values by correcting for inelasticity as described in the text.

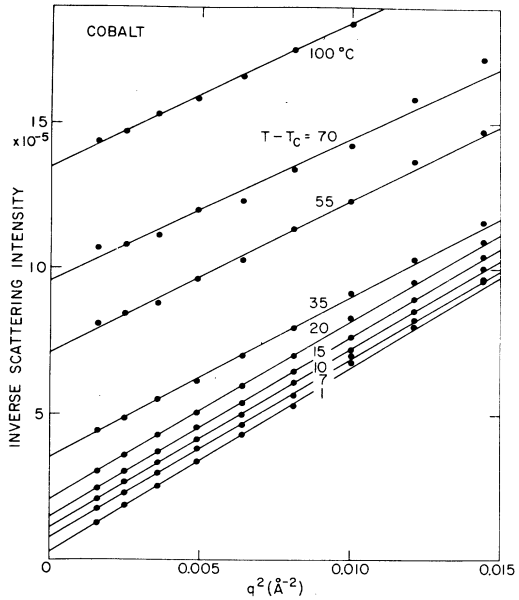

FIG. 9. Reciprocal total scattering intensities for angular scans up to 100 °C above T_C plotted versus q^2 after correcting for inelasticity and resolution effects.

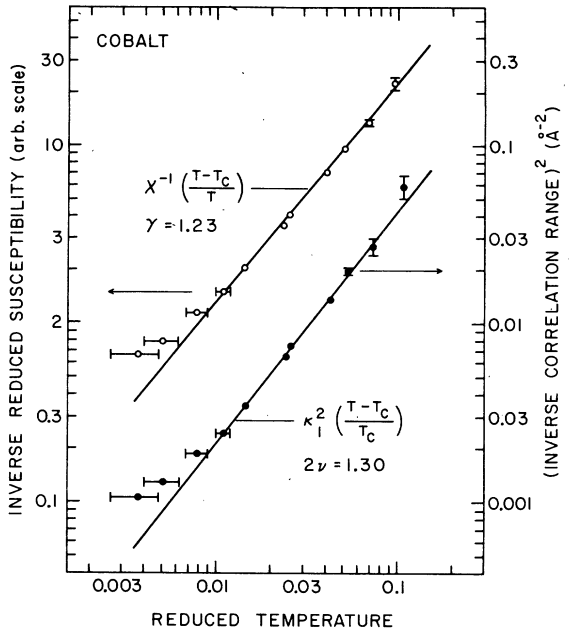

FIG. 10. Temperature dependence of the inverse reduced susceptibility and the square of the inverse correlation range plotted on a log-log scale. The slopes of the fitted straight lines give the exponents γ and 2ν.

In Fig. 9, corrected inverse intensities are plotted versus q^2 for two-axis scans taken at temperatures up to 100 °C above T_C. That all these data are satisfactorily described by the Ornstein-Zernike expression for $\hat{\chi}(q)$ serves to justify its use in computing the inelasticity corrections.

The necessity for making rather large inelasticity corrections to our two-axis data unfortunately precludes our discriminating between the Ornstein-Zernike expression for $\hat{\chi}(q)$ and the slightly modified form proposed by Ritchie and Fisher[19] for example. The uncertainties introduced in the data points in Fig. 9 by correcting for resolution and inelasticity are too large to justify invoking one of the modified expressions to account for any apparent deviations from pure Ornstein-Zernike behavior seen there.

From the data in Fig. 9 we obtain the temperature dependence of the macroscopic susceptibility $\hat{\chi}(q=0)$ and the inverse correlation range κ_1. Since the corrected two-axis intensities in the figure are directly proportional to $\hat{\chi}(q)$, the intercepts of the $1/I$ plots at $q=0$ are therefore proportional to $\hat{\chi}^{-1}(q=0)$ while the extrapolated intercepts with the q^2 axis give κ_1^2 directly. Values for $\hat{\chi}^{-1}(q=0)$ and κ_1^2 obtained in this way are plotted versus reduced temperature on a log-log scale in Fig. 10. Carrying out a weighted least-squares fit of the data for $\hat{\chi}^{-1}(0)$ to the expression,

$$\hat{\chi}^{-1}(q=0) \propto \left(\frac{T-T_C}{T}\right)^{\gamma} \tag{4.6}$$

gives for the exponent γ,

$$\gamma = 1.23 \pm 0.05 . \tag{4.7}$$

By fitting the data for κ_1^2 to the power law,

$$a_{nn}\kappa_1 = F\left(\frac{T-T_C}{T_C}\right)^{\nu}, \tag{4.8}$$

where $a_{nn} = 2.55$ Å is the nearest-neighbor distance for cobalt at T_C, we obtain

$$\begin{aligned} \nu &= 0.65 \pm 0.04 , \\ F &= 2.4 \pm 0.2 . \end{aligned} \tag{4.9}$$

The values we obtain for the exponents γ and ν agree reasonalby well with previous determinations (see Tables I and II). They are, however, significantly lower than the values $\gamma = 1.38$, $\nu = 0.70$ obtained by series expansion calculations[19] for the isotropic Heisenberg model and are much closer to the values $\gamma = 1.24$, $\nu = 0.64$ calculated for the three-dimensional Ising model[18] using the same computational techniques.

Theoretical values for the coefficient F in Eq. (4.8) range from about 2.0 to 2.5. For example, from molecular-field theory[44] $F = 2.45$, for the three-dimensional Ising model[18] $F = 2.30$, and for the Heisenberg model[19] $F = 2.19$. Our experimental value for F is in line with all of the above predictions but is not determined with sufficient precision to discriminate among them.

The one disturbing feature of our data, which can be seen in Fig. 10, is the systematic departure

TABLE I. Values for the exponent γ describing the power-law divergence of the uniform susceptibility above T_C, for iron, cobalt, and nickel.

Material	References	γ
Fe	(56) Noakes *et al.*	1.33 ± 0.015
	(57) Develey	1.33 ± 0.03
	(58) Arajs and Colvin	1.33
	(6) Passell *et al.*[a]	1.30 ± 0.04
	(7) Bally *et al.*[a]	1.34 ± 0.04
Co	(1) Colvin and Arajs	1.21 ± 0.04
	(2) Geissler and Lange	1.20 ± 0.04
	(59) Develey	1.32 ± 0.02
	(3) Rocker and Kohlhass	1.20 ± 0.05
	(5) Bally *et al.*[a]	1.19
	this work[a]	1.23 ± 0.05
Ni	(60) Kouvel *et al.*	1.34 ± 0.01
	(57) Develey	1.32 ± 0.02
	(61) Arajs	1.29 ± 0.04
	(62) Jacrot[a]	1.30

[a]Neutron scattering measurements.

from simple-power-law behavior of the values for κ_1^2 and $\hat{\chi}^{-1}(q=0)$ derived from our measurements closest to T_C. In seeking the origin of this departure, a number of possible causes were considered including multiple scattering and the consequences of a finite value for the Fisher exponent[17] η. The effects of multiple scattering were investigated by means of a Monte Carlo simulation of the experiment in which absorption ($\sigma_{abs} = 52$ b for 13.5 meV neutrons), incoherent scattering ($\sigma_{incoh} = 5.9$ b), and critical scattering were considered as the three most likely processes whereby a neutron can interact with cobalt near T_C.

The overall effect of multiple scattering is to flatten and broaden the critical scattering so that fitting to a Lorentzian shape for $\hat{\chi}(q) \propto (q^2+\kappa_1^2)^{-1}$ leads to an apparent value for κ_1 which is larger than the true value, i.e., the value one would obtain if only singly scattered neutrons were detected. This effect becomes more pronounced close to T_C and will produce systematic errors in the derived values for κ_1 in the same sense as the observed deviations in Fig. 10.[45] However, our computer analysis reveals that, primarily as a result of using a thin sample having a rather large absorption cross-section, the number of neutrons multiply scattered into the angular range of our measurements never exceeds 1% of the total. Shifts in the apparent value of κ_1 cuased by this low level of multiple scattering, while not entirely negligible, can account for only a small fraction of the departure from power-law behavior seen in Fig. 10. Hence multiple scattering cannot be deemed as solely responsible for the curvature in our data.

TABLE II. Previous determinations of the exponent β, describing the power-law temperature dependence of the spontaneous magnetization near T_C, for iron, cobalt, and nickel.

Material	References	β
Fe	(63) Arajs *et al.*	0.389 ± 0.005
	(64) Preston *et al.*	0.34 ± 0.04
	(65) Potter	0.35 ± 0.06
Co	(3) Rocker and Kohlhaas	0.42 ± 0.01
	(4) Myers and Sucksmith	~0.41
Ni	(60) Kouvel *et al.*	0.378 ± 0.004
	(66) Howard *et al.*	0.375 ± 0.02
	(67) Anderson *et al.*	0.35 ± 0.01

To determine if a finite value for η could be responsible for the breakdown in power-law behavior seen in Fig. 10 we attempted to fit our plots of inverse intensity versus q^2 shown in Fig. 9 to the expression[17]

$$1/\hat{\chi}'(q) \propto (\kappa_1^2+q^2)^{1-\eta/2}, \tag{4.10}$$

which is the simplest of the proposed generalizations of the Ornstein-Zernike theory. To deduce a number for η, we imposed the additional constraint that the values of $1/\hat{\chi}'(0)$, obtained by evaluating Eq. (4.10) at $q=0$, obey a power-law temperature dependence. We were, however, unable to fulfill this constraint and also satisfactorily fit our inverse intensity versus q^2 data for any value of η.

We have not been able to attribute the departure from power-law behavior seen in Fig. 10 to any single cause. We note that Bally *et al.*[5] observed no similar breakdown in power-law behavior in their neutron studies on cobalt.

C. Absolute cross-section measurement

In order to determine the so-called interaction range r_1, which appears in the Ornstein-Zernike and other expressions for $\hat{\chi}(q)$, measurements of the wave-vector-dependent susceptibility must be put on an absolute scale. For this reason there have been relatively few experimental determinations of r_1 and among those which have been made, mostly for iron,[46-48] agreement has been poor. This is no doubt due to the difficulties inherent in normalizing the scattering against that from a sample whose cross section is well known, which has been the usual procedure. For cobalt, however, the critical scattering may be calibrated directly against the rather large and accurately measured[49] nuclear spin-incoherent cross section ($\sigma_{incoh} = 5.9$ b) of cobalt itself. In this way factors of sample volume, for example, exactly cancel when forming intensity ratios. Furthermore, the nuclear incoherent scattering is easily separated from the magnetic scattering simply by measuring the forward scattering at low temperatures where there

is no magnetic scattering over the angular range of our two-axis scans. This is due to the extreme steepness of the spin-wave dispersion in cobalt, as discussed in Sec. IV A. Hence the circumstances of our experiment are well suited for an accurate determination of r_1.

The details of our absolute cross-section measurement have been discussed in Ref. 13(b). Here, we merely note that the value we obtained for the ratio of r_1 to the nearest-neighbor distance, $r_1/a_{nn} = 0.46 \pm 0.03$, agrees well with theoretical predictions, which have proven to be rather insensitive both to methods of calculation and to the crystal lattice. For example, the mean-field approximation leads to the result[44] that $r_1/a_{nn} = 0.408$. Ritchie and Fishers's calculations[19] based on the Heisenberg model yield values for r_1/a_{nn} ranging from 0.45 to 0.52 depending on the spin and type of lattice; for a spin-1 system on a fcc lattice, which is the case most applicable to cobalt, they find $r_1/a_{nn} = 0.462$. Similar calculations[18] for the spin-$\frac{1}{2}$ Ising model lead to values for r_1/a_{nn} from 0.44 to 0.46, the former number applying to a fcc lattice.

D. Inelastic scattering above T_C

In this section we present the results of triple-axis, constant-q scans taken at temperature equal to and greater than T_C. These measurements served not only to characterize the dynamics of the spin fluctuations above T_C, but also provided the basis for making the inelasticity corrections to our two-axis data discussed in Sec. IV B.

In Fig. 11, the results of constant-q scans at $q = 0.07$ Å^{-1} are shown for various temperatures both above and below T_C. Figure 11 essentially summarizes the different types of line shapes observed in our triple-axis scans. At T_C, the spin waves have coalesced into a single albeit broadened and round-topped peak. As the temperature is increased above T_C, the line shapes quickly become more obviously single peaked in character. Most noteworthy, however, is the pronounced narrowing of the linewidths with increasing temperature and their subsequent broadening upon approaching the hydrodynamic region. We will return to this point later in this section.

In fitting to the line shapes observed at T_C, a variety of expressions for $F(q,\omega)$ were tried in an effort to best characterize the intrinsic line shape and to extract the q dependence of the characteristic frequency. Single and double-peaked Gaussian and Lorentzian functions, along with the Hubbard line shape discussed in Sec. II C (Fig. 1), were tried as representations for $F(q,\omega)$. Partially as a result of being unable to observe the high-energy tails of the line shapes in our constant-q scans,

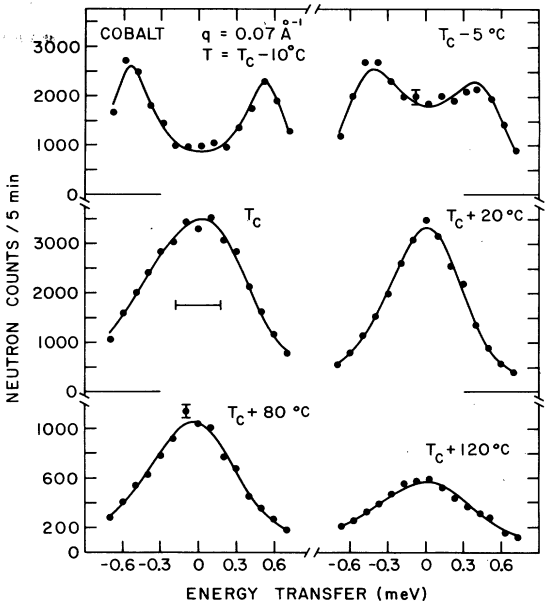

FIG. 11. Energy distribution of the scattering at $q = 0.07$ Å^{-1} on passing through the transition temperature. The curves in the figure were obtained by folding the neutron cross section with the instrument resolution function. The double-ended bar below the curve at T_C indicates the width of the instrument resolution.

satisfactory fits to the data could be obtained for most of the assumed forms for $F(q,\omega)$ in the sense that the χ-squared criterion for the goodness of fit did not strongly favor one form over another.

In fitting to the data at T_C, both the width of $F(q,\omega)$, and an overall scale factor were varied by the fitting program. For the proper expressions for $\hat{\chi}(q)$ [50] and $F(q,\omega)$, this scale factor should be independent of q and hence can serve as an additional criterion, along with the χ-squared test, for judging the appropriateness of a particular choice for $F(q,\omega)$. Among the several expressions for $F(q,\omega)$ which provided satisfactory fits to the observed line shapes, only a single Gaussian and the Hubbard line shapes also met this second criterion. Overall, values for χ-squared were somewhat lower for the fits obtained with a Gaussian rather than the Hubbard form for $F(q,\omega)$ as best representing our data at T_C.

The half-width at half-maximum energies derived from our data at T_C by fitting to a Gaussian $F(q,\omega)$ are plotted in Fig. 12. The exponent obtained for the q-dependence of the intrinsic widths of the Gaussian fits is 2.4 ± 0.2. The dashed line in Fig. 12 has a slope of 2.5, the value predicted from dynamical scaling for the q-dependence of the characteristic frequency at T_C. Fitting to the Hubbard form for $F(q,\omega)$ resulted in an exponent of 2.2, however, which indicates that the value de-

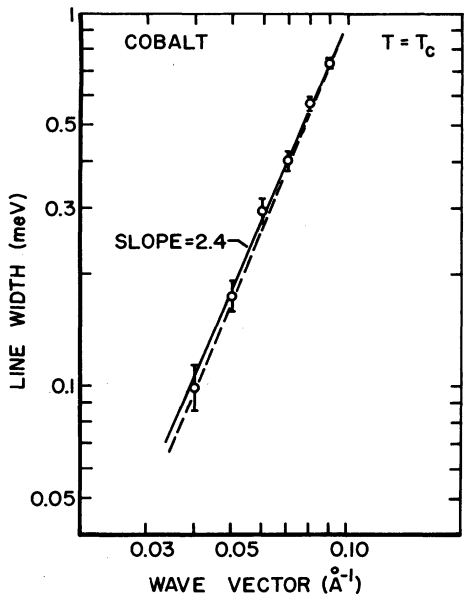

FIG. 12. Half-width at half-maximum energies derived from fitting the line shapes observed in constant-Q scans at T_C with a Gaussian spectral-weight function. The slope of the fitted line gives the q-dependence of the linewidths. The dashed line has a slope of 2.5, the value predicted by scaling.

rived for the exponent is rather sensitive to the choice of spectral shape function used in the analysis.

As can be seen from Fig. 12, our data are certainly consistent with the $\frac{5}{2}$ power law predicted by dynamical scaling. If we assume a $\frac{5}{2}$ law, then the half widths at half maximum of our line shape at T_C are best described by the relation

$$\Gamma(q, \kappa_1 = 0) = 300\, q^{5/2}\,\text{meV}\,. \tag{4.11}$$

It is Eq. (4.11) which is plotted as the dashed line in Fig. 12. The coefficient, 300 ± 30 meV Å$^{5/2}$, is a measure of the overall degree of inelasticity of the critical scattering and is quite large for cobalt. The corresponding value for iron[10] is only 130 meV Å$^{5/2}$, for example.

For our inelastic scattering data above T_C, both Lorentzian and Gaussian forms for $F(q, \omega)$ were convoluted with the spectrometer resolution function and fit to the observed line shapes. The Hubbard form for $F(q, \omega)$ was not employed in fitting to these data, however, because over the temperature range of most of our measurements the Hubbard form differs little from a simple Lorentzian. In contrast to the results at T_C, the least-squares fits obtained with a Lorentzian shape were consistently better, both in the sense of having lower χ-squared values and a normalization factor which showed no q dependence, than the Gaussian fits.

Consequently, the characteristic frequencies of the inelastic scattering above T_C were taken to be the intrinsic half-widths at half-maximum of the fitted Lorentzian line shapes.

From our measurements of the characteristic frequency at general values of wave vector and temperature above T_C, we have been able to test directly one of the cardinal assumptions of dynamical scaling; namely, that the characteristic frequency is a homogeneous function of q and κ_1 of the form

$$\Gamma(q, \kappa_1) = \sigma q^{5/2} \Omega(\kappa_1/q)\,, \tag{4.12}$$

where the scaling function $\Omega(\kappa_1/q)$ is normalized to unity for $\kappa_1/q = 0$ and has the limiting behavior $\Omega(\kappa_1/q) \propto (\kappa_1/q)^{1/2}$ for $\kappa_1 \gg q$ in accord with hydrodynamic theory.[23] We have already seen that for cobalt the linewidths at T_C are adequately described by the expression $\Gamma(q, 0) = \sigma q^{5/2}$, with $\sigma = 300$ meV Å$^{5/2}$. Hence the ratios, $\Gamma(q, \kappa_1)/\sigma q^{5/2}$, of the linewidths above T_C to those at T_C, when plotted as a function of κ_1/q, should lie on a single curve which would then serve to empirically determine the form of the scaling function $\Omega(\kappa_1/q)$.

Using the values of κ_1 derived from our corrected two-axis data [Eqs. (4.8) and (4.9)], we have plotted the linewidth ratios[51] obtained from our triple-axis measurements as a function of κ_1/q in Fig. 13. There we find that, within the experimental uncertainties, the linewidth ratios do indeed lie on a single curve as anticipated by dynamical scaling.

The dashed curve in Fig. 13 is a calculation of the scaling function $\Omega(\kappa_1/q)$ for a Heisenberg ferromagnet by Resibois and Piette[52] who solved, in a lowest-order approximation, the kinetic equations obtained by DeLeener and Resibois[53] and by Kawasaki.[54] Although in overall agreement with Resibois and Piette's result, the data in the figure show a deeper minimum, shifted to a lower value

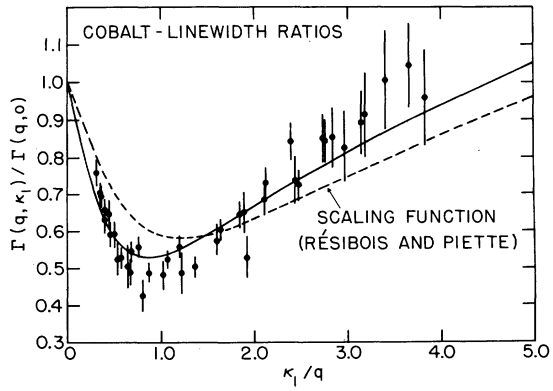

FIG. 13. Shape of the dynamical scaling function for cobalt obtained by plotting the ratios of the linewidths above T_C to those at T_C as a function of κ_1/q.

of κ_1/q, followed by a more rapid broadening of the linewidths than is accounted for by their calculation. The linewidths derived from Hubbard's calculation of the full spectral-weight function show a narrowing from 50% to 60% near $\kappa_1/q=1$ which would seem to agree well with our observed linewidths. However, full details of the shape of the scaling function implicit in Hubbard's results, particularly at larger κ_1/q, have not been published.

The Resibois-Piette result for the scaling function $\Omega(\kappa_1/q)$, although obtainable only by iterative, numerical methods, is rather closely approximated by the simple expression

$$\Omega(\kappa_1/q)\simeq e^{-1.83\kappa_1/q}+0.43(\kappa_1/q)^{1/2}\ \text{(Résibois-Piette)}. \tag{4.13}$$

The solid curve in Fig. 13 was obtained by varying the constants in the above equation in a weighted least-squares fit to our data which gave the result

$$\Omega(\kappa_1/q)=e^{-2.74\kappa_1/q}+0.47(\kappa_1/q)^{1/2}. \tag{4.14}$$

Equation (4.14), in conjunction with Eq. (4.12), was used to analytically describe the inelasticity of the critical scattering in making the corrections to our two-axis data described in Sec. IV B.

Since our linewidth measurements extended out to nearly $\kappa_1/q=4$, it was hoped that sufficient data had been collected within the hydrodynamic regime to enable the power-law temperature dependence of the spin diffusion constant Λ to be determined. The linewidths extracted from data taken at temperatures greater than 80° above T_C did indeed exhibit the q^2 dependence indicative of spin diffusion (i.e., $\Gamma=\Lambda q^2$). From these data, only those linewidths obtained at wave vectors such that $\kappa_1/q\geq 2$ were considered in computing values for Λ from the slopes of Γ vs q^2 plots. In this way values of Λ were obtained for reduced temperatures from $(T-T_C)/T_C=0.06$ to 0.11. When plotted versus reduced temperature on a log-log scale, however, our derived values for Λ failed to lie on a straight line but rather showed a systematic curvature. The local slope at the highest temperatures was about $\frac{1}{3}$, the values expected from the hydrodynamic prediction that $\Lambda\propto\kappa_1^{1/2}\propto(T-T_C)^{\nu/2}$, but steepened to more than $\frac{1}{2}$ at the lower temperatures. This departure from expected hydrodynamic behavior is similar to that observed by Parette and Kahn[55] in their neutron time-of-flight study of spin diffusion in iron. They found anomalous exponents for the temperature dependence of Λ for data corresponding to $1<\kappa_1/q<4$, a region they termed "quasihydrodynamic," and were able to observe the predicted hydrodynamic behavior only in the region $\kappa_1/q>4$. Our data are consistent with their conclusion that the crossover from critical to hydrodynamic regimes is quite gradual so that κ_1/q must be large before true hydrodynamic behavior may be observed.

V. CONCLUSIONS AND COMPARISON WITH IRON AND NICKEL

Our neutron scattering studies have shown cobalt to be an example of a magnetic system whose critical scattering exhibits a high degree of inelasticity. The linewidths we observed for cobalt are, for example, more than twice as broad as those in iron.[8,10] The effect of the inelasticity is to cause the angular distributions of the critical scattering to deviate significantly from the expected behavior of the static susceptibility $\chi(q)$. However, by empirically determining the form of the spectral weight function $F(q,\omega)$ through a separate series of triple-axis measurements, the inelasticity effects could be removed from our data, at least above T_C. We find that above T_C the Ornstein-Zernike expression for $\chi(q)$ provides an adequate description of the wave-vector dependence of the critical scattering. Below T_C, however, we have not been able to separate transverse and longitudinal components of the susceptibility. In fact, we find clear evidence for only the transverse component. The form of the longitudinal susceptibility below T_C is for cobalt, as well as for all other isotropic ferromagnets investigated so far, the least understood aspect of the critical scattering.

With regard to the dynamics, we find that the hydrodynamic expression of Halperin and Hohenberg for the transverse spectral shape function $F^t(q,\omega)$ describes our inelastic scattering line shapes at all temperatures below T_C. At T_C we observe a single peaked spectral function with an approximately Gaussian shape which quickly becomes Lorentzian in character at higher temperatures. The highly inelastic nature of the critical scattering in cobalt enabled us to make accurate linewidth measurements above T_C and thereby deduce the form of the dynamical scaling function. Our results for cobalt show some significant deviation from the scaling function calculated by Résibois and Piette for a simple Heisenberg ferromagnet which has been found to give a highly successful account of the inelastic scattering in iron.[10,55]

We have noted above and in previous sections some of the similarities and differences between our results for cobalt and those for iron and nickel. Here we summarize the current situation regarding the critical behavior of the transition-metal ferromagnets by presenting tables of results of a variety of measurements, emphasizing those quan-

TABLE III. Values for the coefficient F and exponent ν in the expression $a_{nn}\kappa_1 = F(T/T_C - 1)^{\nu}$ describing the power law behavior of the inverse correlation function above T_C, and also Fisher's exponent η, for iron, cobalt, and nickel.

Material	References	F	ν	η
Fe	(7) Bally *et al.*	2.97 ±0.15	0.70 ±0.015	0.07 ±0.05
Co	(5) Bally *et al.*	~1.17	0.625	0.10 ±0.05
	this work	2.4 ±0.2	0.65 ±0.04	...
Ni		...	...	...

tities which are accessible to measurement by neutron scattering.

The critical exponent γ, giving the degree of the divergence of the uniform susceptibility above T_C, has received the greatest attention in experimental investigations of the critical behavior of the transition-metal ferromagnets. Some of the more recent results for γ are listed in Table I. We note that there is basic agreement between the values for γ measured by neutron scattering and those determined by bulk techniques. There is also basic agreement between the values for γ obtained for iron and nickel which range from 1.30 to 1.34. These values are somewhat lower than the most recent numerical estimates[19] of γ obtained for the Heisenberg model which give $\gamma = 1.38 \pm 0.02$. On the other hand, all of the susceptibility measurements for cobalt, with the exception of Develey's,[59] place the value of γ near 1.2.

It is interesting to compare the values for γ listed in Table I with those for the exponent β, which describes the power-law behavior of the spontaneous magnetization near T_C. These are listed in Table II. Once again the results for iron and nickel are seen to be quite similar and in this case agree reasonably well with the theoretical estimate[42] that $\beta \simeq 0.38$ obtained for the Heisenberg model. There has been only one direct measurement of β for cobalt, that of Rocker and Kohlhaas[3] who obtained $\beta = 0.42 \pm 0.01$. This result receives support from the magnetization measurements of Myers and Sucksmith,[4] however, which extended to within 0.995 T_C. The data of Myers and Sucksmith, when plotted versus $|T - T_C|$ on a log-log scale is linear near T_C and yields a value for β of ~0.41. Hence these two results would again indicate a departure in the critical behavior of cobalt from that of iron and nickel. The values of γ and β for cobalt both deviate from iron and nickel in the same sense; i.e., toward the mean-field exponents $\gamma = 1$, $\beta = \frac{1}{2}$.

We continue our comparison of the static critical properties of iron, cobalt and nickel in Table III where values for the exponent ν, describing the power-law behavior of the inverse correlation range κ_1, and for Fisher's exponent η are listed. Although there have been a number of early critical scattering studies of iron which have focused on the asymptotic form of the spin correlation function, the actual power-law dependence of κ_1 was seldom extracted from such measurements. Furthermore, the effects of the inelasticity of the scattering on the apparent value of κ_1 were not well-understood and often not taken into account in these early experiments. Bally's results for ν and η listed in Table III were obtained after correcting for inelasticity, although this was done in an approximate manner since the full form of the dynamical scaling function for iron was not known at that time. These results for iron are in good agreement with predictions based on the Heisenberg model[19] that $\nu \simeq 0.70$ and $\eta \simeq 0.04$.

For cobalt, we note that in Table III there is some disagreement between our results and those of Bally *et al.*, particularly with regard to the coefficient F which measures the absolute magnitude of κ_1. Since information on the dynamics of the spin fluctuations in cobalt was not available at the time of Bally's work, he assumed that the inelasticity corrections required for cobalt would be about the same as those for iron. Our inelastic scattering measurements have shown, however, that the critical scattering in cobalt is far more inelastic than that for iron, contradicting Bally's assumption. This is the probable origin of the differences seen in Table III between Bally's results and our own. Nevertheless, both values for ν are somewhat lower than that found for iron and again deviate from the Heisenberg model result in the direction of the mean-field value $\nu = \frac{1}{2}$.

According to scaling, the exponents β, ν, and γ are not all independent quantities but are, in fact, related through the expression $\beta = \frac{1}{2}(3\nu - \gamma)$. We can test this relation for both iron and cobalt by using the highest precision values for the exponents given in the foregoing tables. Hence for iron we use $\beta = 0.389 \pm 0.005$,[63] $\nu = 0.70 \pm 0.015$,[7] and $\gamma = 1.333 \pm 0.015$.[56] For cobalt we take $\beta = 0.42 \pm 0.01$,[3] together with our own results for ν and γ. For these exponent values we obtain

TABLE IV. Values of dynamical critical exponents for iron, cobalt, and nickel determined by neutron scattering.

Dynamical property	Expression	Scaling laws	Heisenberg model	Iron	Cobalt [a]	Nickel [b]
Linewidth at T_C	$\Gamma \sim q^z$	$z = \frac{5}{2} - \frac{1}{2}\eta$	~2.48	2.7 ±0.3 [c] 2.8 ±0.3 [d]	2.4 ±0.2	2.46 ±0.25
Spin-wave stiffness	$D \sim (1 - T/T_C)^x$	$x = \nu' - \beta$	~0.32	0.37 ±0.03 [c] 0.36 ±0.03 [d]	0.39 ±0.05	0.39 ±0.04
Spin diffusion constant	$\Lambda \sim (T/T_C - 1)^y$	$y = (\nu/\nu')(\nu' - \beta)$	~0.32	0.38 ±0.06 [e]	...	...

[a] This work.
[b] Reference 12.
[c] Reference 8.
[d] Reference 26.
[e] Reference 55.

$$\beta - (3\nu - \gamma)/2 = \begin{cases} +0.005 \pm 0.02 \text{ for iron}, \\ +0.06 \pm 0.07 \text{ for cobalt}. \end{cases}$$

Hence although the values for the exponents β, ν, and γ are different for iron and cobalt, the scaling law relating these exponents is found to be satisfied, to within the experimental uncertainties, for both materials.

Turning now to the dynamical properties, we compare in Table IV the results of inelastic neutron scattering measurements on iron, cobalt, and nickel with scaling predictions. We see that there is satisfactory agreement for all three materials with the prediction that at T_C the characteristic frequency varies with q to about the $\frac{5}{2}$ power. The coefficient of the $\frac{5}{2}$ law is a measure of the overall degree of inelasticity of the critical scattering. For cobalt we find for this coefficient $\sigma = 300 \pm 30$ meV Å$^{5/2}$ compared to $\sigma = 130$ meV Å$^{5/2}$ for iron and $\sigma \simeq 330$ meV Å$^{5/2}$ for nickel, indicating that the critical scattering in nickel is even more inelastic than that for cobalt.

Reasonably consistent results have also been found for the power-law dependence of the spin-wave stiffness constant D in all three materials, although the experimental uncertainties are rather large. Scaling predicts that D should vary with $|T - T_C|$ to the $\nu' - \beta$ power. If we use the static scaling result that $\nu' = \nu$ and the values for ν and β for cobalt listed in the preceding tables, this leads to an exponent for D of only ~0.23, far below what we actually observed. However, it may be inappropriate to assume that $\nu' = \nu$ since the longitudinal susceptibility below T_C has never been clearly identified in these materials. It is therefore not clear what meaning should be attributed to the exponent ν'. The results in Table IV would suggest rather that D scales directly with the magnetization although more precise measurements are needed to confirm this speculation.

The experimental results regarding the power-law behavior of the spin diffusion constant are unfortunately quite limited. Our triple-axis measurements above T_C support the conclusion drawn by Parette and Kahn[55] from their spin diffusion studies in iron that the true hydrodynamic regime above T_C lies beyond $\kappa_1/q \sim 4$. Earlier neutron-scattering measurements of the spin diffusion in iron[8] and nickel[12] were probably not made entirely within the hydrodynamic region and therefore the anomalous exponents obtained for the spin diffusion constant in these studies must be discounted. Parette and Kahn did claim to succeed in reaching the hydrodynamic region in their time-of-flight measurements on iron and their result in Table IV gives the only indication at present that the spin diffusion processes in the transition metals are correctly described by hydrodynamics.

From the foregoing tables and discussion, it is evident that a complete phenomenological description of the critical behavior of the transition metal ferromagnets does not yet exist. Further investigation is needed, especially in the case of nickel. The form of the dynamical scaling function for nickel has not yet been determined. Since the critical scattering in nickel is even more inelastic than that for cobalt, the scaling function for nickel is of particular interest.

ACKNOWLEDGMENTS

Two of the authors (C.J.G. and V.J.M.) wish to acknowledge the support and hospitality extended by Brookhaven National Laboratory during the course of this work. We also wish to thank W. E. Lenz, J. J. Hurst, and P. E. Pyne for their expert technical assistance.

*Work supported by the NSF.
†Guest scientist at Brookhaven National Laboratory.
‡Present address: National Bureau of Standards, Washington, D. C. 20234.
§Present address: IBM Research Center, San Jose, Calif. 95193.
||Work at Brookhaven supported by ERDA.

[1]R. V. Colvin and S. Arajs, J. Phys. Chem. Solids 26, 435 (1965).
[2]K. K. Geissler and H. Lange, Z. Angew. Phys. 21, 357 (1966).
[3]W. Rocker and R. Kohlhass, Z. Naturforsch. A 22, 291 (1967).
[4]H. P. Myers and W. Sucksmith, Proc. R. Soc. Lond. 207A, 427 (1951).
[5]D. Bally, M. Popovici, M. Totia, B. Grabcev, and A. M. Lungu, *Neutron Inelastic Scattering* (IAEA, Copenhagen, 1968), Vol. II, p. 75.
[6]L. Passell, K. Blinowski, T. Brun, and P. Nielsen, Phys. Rev. 139, A1866 (1965).
[7]D. Bally, M. Popovici, M. Totia, B. Grabcev, and A. M. Lungu, Phys. Lett. 26A, 396 (1968).
[8]M. F. Collins, V. J. Minkiewicz, R. Nathans, L. Passell, and G. Shirane, Phys. Rev. 179, 417 (1969).
[9]A. Tucciarone, H. Y. Lau, L. M. Corliss, A. Delapalme, and J. M. Hastings, Phys. Rev. B 4, 3206 (1971).
[10]J. Als-Nielsen, Phys. Rev. Lett. 25, 730 (1970).
[11]D. S. Rodbell, Physics 1, 279 (1965).
[12]V. J. Minkiewicz, M. F. Collins, R. Nathans, and G. Shirane, Phys. Rev. 182, 624 (1969).
[13]C. J. Glinka, V. J. Minkiewicz and L. Passell, AIP Conf. Proc. 24, 283 (1975); 29, 499 (1976).
[14]W. Marshall and S. W. Lovesey, *Theory of Thermal Neutron Scattering* (Oxford U. P., London, 1971).
[15]R. Kubo, J. Phys. Soc. Jpn. 12, 570 (1957).
[16]For example, M. S. Green, J. Chem. Phys. 33, 1403 (1960).
[17]M. E. Fisher, J. Math. Phys. 5, 944 (1964).
[18]M. E. Fisher and R. J. Burford, Phys. Rev. 156, 583 (1967).
[19]D. S. Ritchie and M. E. Fisher, Phys. Rev. B 5, 2668 (1972).
[20]K. Kawasaki, Prog. Theor. Phys. 38, 1052 (1967).
[21]J. Als-Nielsen, O. W. Dietrich, and L. Passell, Phys. Rev. 14, 4908 (1976).
[22]F. J. Dyson, Phys. Rev. 102, 1217 (1956); 102, 1230 (1956).
[23]B. I. Halperin and P. C. Hohenberg, Phys. Rev. Lett. 19, 700 (1967); Phys. Rev. 177, 952 (1969).
[24]M. P. Schulhof, P. Heller, R. Nathans and A. Linz, Phys. Rev. B 1, 2304 (1970).
[25]V. J. Minkiewicz, K. Gesi and E. Hirahara, J. Appl. Phys. 42, 1374 (1971).
[26]S. Boronkay and M. F. Collins, Int. J. Mag. 4, 205 (1973).
[27]L. Passell, J. Als-Nielsen, and O. W. Dietrich, *Neutron Inelastic Scattering* (IAEA, Vienna, 1972), p. 619.
[28]G. Shirane and J. Als-Nielsen, Proc. ICM (Moscow) II, 255 (1973).
[29]M. Iizumi, J. Lynn, A. Ohsawa, and H. Ito, AIP Conf. Proc. 29, 266 (1976).
[30]V. G. Vaks, A. I. Larkin, and S. A. Pikin, Sov. Phys.-JETP 26, 188 (1968); 26, 647 (1968).
[31]L. Van Hove, Phys. Rev. 95, 1374 (1954).
[32]B. Widom, J. Chem. Phys. 43, 3892 (1965); 43, 3898 (1965).
[33]L. P. Kadanoff, Physics 2, 263 (1966).
[34]J. W. Essam and M. E. Fisher, J. Chem. Phys. 39, 842 (1963); M. E. Fisher, J. Appl. Phys. 38, 981 (1967); C. Domb and D. L. Hunter, Proc. Phys. Soc. Lond. 86, 1147 (1965).
[35]R. A. Ferrell, N. Menyhard, H. Schmidt, F. Schwabl, and P. Szepfalusy, Phys. Rev. Lett. 18, 891 (1967); Ann. Phys. (N.Y.) 47, 565 (1968).
[36]Actually, hydrodynamic theory together with static scaling lead to the result that $D \propto \kappa^{1-\beta/\nu'}$. To illustrate the application of dynamical scaling we have let $\beta = \frac{1}{3}$ and $\nu' = \nu = \frac{2}{3}$.
[37]J. Hubbard, J. Phys. C 4, 53 (1971).
[38]H. Mori, Prog. Theor. Phys. 33, 423 (1965).
[39]K. Kawasaki, J. Phys. Chem. Solids 28, 1277 (1967); Prog. Theor, Phys. (Kyoto) 39, 285 (1968).
[40]P. Résibois and M. DeLeener, Phys. 152, 305 (1968); F. Wegner, Z. Phys. 216, 433 (1968); M. Blume and J. Hubbard, Phys. Rev. B 1, 3815 (1970).
[41]S. J. Pickart and H. A. Alperin, Phys. Rev. 156, 623 (1967).
[42]R. L. Stephenson and P. J. Wood, J. Phys. C 3, 90 (1970).
[43]P. Nielsen, Risö Technical Report No. 118 (1965) (unpublished).
[44]P. G. DeGennes and A. Herpin, C. R. Acad. Sci. B 243, 1611 (1956).
[45]This result has also been obtained in a recent, more fundamental, analysis of the effects of multiple scattering on critical scattering data by W. A. Holm and H. A. Gersch [Phys. Rev. B 13, 4984 (1976)].
[46]H. A. Gersch, C. G. Shull, and M. K. Wilkinson, Phys. Rev. 103, 525 (1956).
[47]M. Ericson and B. Jacrot, Phys. Chem. Solids 13, 235 (1960).
[48]S. Spooner and B. L. Averbach, Phys. Rev. 142, 291 (1966).
[49]R. I. Schermer, Phys. Rev. 130, 1907 (1963).
[50]The Ornstein-Zernike form for $\hat{\chi}(q)$ was used in the fitting routine with κ_1 set equal to zero at T_C.
[51]Ratios of half-height rather than half-area frequencies have been plotted in Fig. 13. While for the Lorentzian line shapes observed above T_C, these two frequencies are equal, this is not the case for a Gaussian line shape such as was found to best describe our data at T_C. Since there is no *a priori* reason for regarding either of these definitions as more "characteristic" of the spin dynamics, we have chosen to plot the half-height ratios since these are in closer agreement with theoretical calculations.
[52]P. Résibois and C. Piette, Phys. Rev. Lett. 24, 514 (1970).
[53]P. Résibois and M. DeLeener, Phys. Lett. 25A, 65 (1967); Phys. Rev. 178, 806 (1969).
[54]K. Kawasaki, Progr. Theor. Phys. (Kyoto) 39, 1133 (1968); 40, 11 (1968); 40, 706 (1968); 40, 930 (1968).
[55]G. Parette and R. Kohn, J. Phys. 32, 447 (1971).
[56]J. E. Noakes, N. Tornberg, and A. Arrott, J. Appl. Phys. 37, 1264 (1966).
[57]G. Develey, C. R. Acad. Sci. (Paris), 260, 4951 (1965).
[58]S. Arajs and R. V. Colvin, J. Appl. Phys. 35, 2424 (1964).
[59]G. Develey, C. R. Acad. Sci. B 262, B103 (1966).

[60]J. S. Kouvel, J. B. Kouvel, and J. B. Comly, Phys. Rev. Lett. 20, 1237 (1968).
[61]S. Arajs, J. Appl. Phys. 36, 1136 (1965).
[62]B. Jacrot, J. Konstantinovic, G. Parette, and D. Cribier, *Inelastic Scattering of Neutrons in Solids and Liquids* (IAEA, Vienna, 1963), Vol. 2.
[63]S. Arajs, B. L. Tehan, E. E. Anderson, and A. A. Stelmach, Int. J. Mag. 1, 41 (1970).
[64]R. S. Preston, S. S. Hanna and J. Heberle, Phys. Rev. 128, 2207 (1962).
[65]H. H. Potter, Proc. R. Soc. A 146, 362 (1934).
[66]D. G. Howard, B. D. Dunlap, and J. G. Dash, Phys. Rev. Lett. 15, 628 (1965).
[67]E. E. Anderson, S. Arajs, A. A. Stelmach, B. L. Tehan, and Y. D. Yao, Phys. Lett. 36A, 173 (1971).